# Vertical Growth of Two-Dimensional Zinc Oxide Nanostructures on ITO-Coated Glass: Effects of Deposition Temperature and Deposition Time

**D. Pradhan and K. T. Leung***

*WATLab and Department of Chemistry, University of Waterloo, Waterloo, Ontario N2L 3G1, Canada*

*Received: August 28, 2007*

Two-dimensional (2D) zinc oxide (ZnO) nanostructures of thickness 40−100 nm and length up to several micrometers are vertically grown on indium−tin oxide-coated glass substrates by using electrochemical deposition in the temperature range of 22−90 °C. The deposition temperature is found to play a significant role in controlling the morphology of the nanostructures, from randomly oriented, poorly crystalline nanosheets at 22 °C to well-aligned nanowalls with wurtzite structure at 70 °C. At 80 °C, nanowalls are found to merge with one another, and they become patchy fibrillar structures at 90 °C. An optical direct band gap of 3.3 eV is measured for all the samples deposited above 50 °C, while their transmittance varies from 40 to 75%, depending on their morphologies. X-ray photoelectron spectroscopy (XPS) shows that the ZnO nanostructures are covered by a $Zn(OH)_2$ overlayer, in good accord with the general growth model that involves $Zn^{2+}$ hydroxylation followed by dehydration to ZnO. Furthermore, our XPS data also reveals the presence of chlorine throughout the ZnO nanostructures, which verifies for the first time the 2D growth mechanism that involves $Cl^-$ capping of the (0001) plane of ZnO and thereby redirecting growth in the $(10\bar{1}0)$ plane. Early growth of nanowalls at 70 °C arising from spherical nanoparticles to elongated nanobars is demonstrated by varying the deposition time.

## 1. Introduction

Zinc oxide (ZnO) is one of the important wide-band-gap, n-type, semiconducting materials with promising applications in sensors, optoelectronic devices, solar cells, and field emitters.[1−4] The properties of ZnO nanostructures highly depend on their shapes, sizes, aspect ratios, orientations, and crystalline densities. In recent years, a variety of ZnO nanostructures, such as nanowires/nanorods, nanotubes, nanobelts, nanosprings, nanohelices, nanorings, nanobows, nanopropellers, nanodisks, and nanoplatelets, have been prepared primarily by using thermal evaporation techniques.[5] In contrast to the rather limited number of studies on two-dimensional (2D) ZnO nanostructures,[6−8] the majority of the work on ZnO are based on the fabrication of quasi one-dimensional (1D) ZnO nanostructures (nanowires, nanopillars, and nanobelts) due to the readily anisotropic ZnO growth along the *c*-axis.[5,9−12] Various techniques, such as thermal evaporation and solution-based chemistry (hydrothermal, solvothermal, sol−gel, and electrochemical deposition), have been used to synthesize these 1D and 2D ZnO nanostructures.[5,9−11,13] In the thermal evaporation method, the use of high temperature (>900 °C) and a Au catalyst is required to synthesize 2D ZnO nanostructures (nanowalls).[8,14] A solution-based chemical approach is therefore more attractive due to the lower-temperature, single-step, catalyst-free growth process and its potential for large scale production. In particular, Liu et al. synthesized hollow ZnO dandelions with single crystalline building units (either nanorods or nanoplatelets) using a modified solution-based Kirkendall process,[15] whereas Tian et al. produced nanoplate stacks using citrate acid in a wet chemistry synthesis.[16] Recently, Kar et al. prepared ZnO nanosheets (and nanowires) by a solvothermal route.[11] To date, despite numerous studies on electrochemical deposition of ZnO nanorods on various substrates, such as GaN,[17] indium−tin oxide (ITO),[13,18,19] $SnO_2$,[20] ZnO films,[21] and Zn foils,[22,23] there are only a few reports on 2D ZnO nanostructures, including nanoplates, nanosheets and nanodisks.[21,24−26] Furthermore, none of these reported 2D nanostructures is found to be vertically grown on the substrate. Vertical 2D nanostructures are particularly interesting not only for extending our understanding of the mechanism of nanostructure growth, but also for developing novel applications in sensors, photocatalysts, nanocontainers, nanoreactors, and templates for 2D structures of other materials.

In the present work, we demonstrate the vertical growth of 2D ZnO nanostructures on ITO-coated glass substrates (ITO-glass) using an electrochemical deposition method. By systematically controlling the electrochemical deposition parameters (electrolyte concentrations, deposition potential, and deposition temperature), it is possible to produce well-defined 2D nanostructures with high alignment and uniformity. Specifically, the deposition temperature can be used to control the morphology of ZnO, from nanosheets to nanowalls. The crystallography and optical properties of these ZnO nanostructures are determined by glancing-incidence X-ray diffraction (GIXRD) and UV−vis spectroscopy, respectively. We also carry out an extensive study by X-ray photoelectron spectroscopy (XPS) to characterize for the first time detailed composition profiles as a function of sputtering depth and to probe the effects of electrolyte components, particularly the important role of the $Cl^-$ ions, on the growth mechanism. Furthermore, on the basis of their morphology evolution as a function of deposition time, we propose a growth model for the early formation of wall-like ZnO nanostructures.

## 2. Experimental Details

The electrochemical deposition experiments were carried out in a conventional three-electrode cell immersed in a water bath

* Corresponding author.

10.1021/jp076890n CCC: $40.75 
Published on Web 01/16/2008

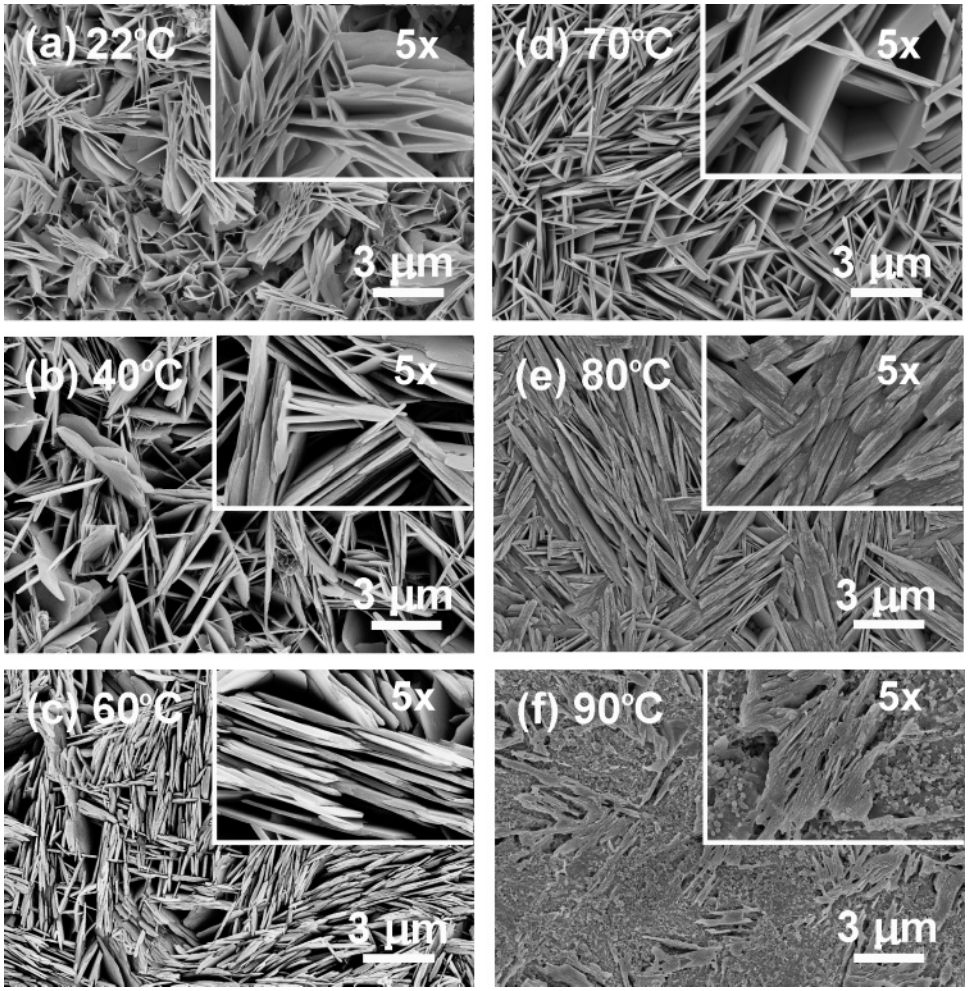


**Figure 1.** SEM images of 2D ZnO nanostructures electrodeposited on ITO-glass at (a) 22, (b) 40, (c) 60, (d) 70, (e) 80, and (f) 90 °C. Insets show the corresponding magnified views of selected sections of the respective images.

at different temperatures (22−90 °C) held constant to within ±1 °C. The working electrode was single-side polished, $SiO_2$-passivated float glass coated with an ITO film (200−500 nm thick, and with a sheet resistance, $R_s$, of 4−8 Ω) obtained from Delta Technologies Limited (Stillwater, MN). The ITO surface was found to be extremely smooth, with a rms roughness of 0.4 nm as measured by atomic force microscopy (Digital Instruments Nanoscope IV). A Ag/AgCl electrode was used as the reference electrode, and a platinum wire served as the counter electrode. A 15 mL solution of 0.1 M zinc nitrate [$Zn(NO_3)_2 \cdot 6H_2O$] mixed with 0.1 M potassium chloride (KCl) (both from Aldrich) was prepared with Millipore water, and the resulting electrolyte solution was stirred for at least 15 min prior to electrodeposition. A potentio-/galvanostat electrochemical workstation (CH Instruments 660A) was used to deposit the ZnO nanostructures by amperometry potentiostatically at −1.1 V (relative to the Ag/AgCl reference electrode). In addition to varying the deposition temperature, the deposition time was changed from 1 to 3600 s at a selected temperature (70 °C) to study its effects on the nucleation and growth behavior of ZnO nanowalls. After deposition, the resulting nanodeposits were thoroughly rinsed in Millipore water and dried under a nitrogen gas stream.

The surface morphology and elemental compositions of ZnO nanodeposits were characterized by using a field-emission scanning electron microscope (FESEM LEO 1530) equipped with an on-system energy-dispersive X-ray (EDX) analysis system (EDAX Pegasus 1200). GIXRD patterns were recorded on a high-resolution four-circle X-ray diffractometer (PANalytical X'Pert Pro MRD) with Cu Kα radiation (1.542 Å) at an incidence angle $\omega = 0.3°$. The optical properties of the ZnO nanostructures were measured with a UV−vis spectrometer (Perkin-Elmer Lambda 35) equipped with an integrating sphere (Labsphere). The surface composition of the ZnO nanostructures was analyzed by XPS (Thermo-VG Scientific ESCALab 250) with a monochromatic Al Kα X-ray source (1486.6 eV). The binding energy (BE) positions, full width at half-maxima (fwhm), and area intensities of individual XPS features were determined by using CasaXPS software with the appropriate Shirley background correction.

## 3. Results and Discussion

**3.1. Evolution of 2D Nanostructures with Deposition Temperature.** Figure 1 shows the SEM images of ZnO nanostructures electrodeposited at different temperatures for 1 h. At 22 °C (ambient temperature), nanosheets resembling flower petals with nonuniform size and thickness in the range of 40−100 nm are obtained (Figure 1a). These petal-like structures appear to distribute randomly as individual sheets not necessarily perpendicular to the substrate. A large fraction of nanosheets form tripe-like networks with pockets and multiple branches along different directions (Figure 1a). This nanosheet morphology is found to be quite similar to that of ZnO nanosheets produced on the surface of Zn foils by heating in ethanol at 200 °C for 3−12 h by Kar et al. using a solvothermal

technique,[11] whereas discoid ZnO microstructures were obtained in a 5 h reaction process by Peng et al. using a polymer controlled crystallization method.[27] In contrast to these synthesis procedures, the present electrochemical deposition could produce ZnO nanosheets in a considerably shorter time (1 h). At a higher deposition temperature of 40 °C (Figure 1b), the ZnO nanosheets become flat platelets with fewer branched networks than those formed at 22 °C. The length and thickness of these nanoplatelets are ~3 $\mu$m and 40−100 nm, respectively. These nanoplatelets appear to have sharp edges, and increasing fractions of the nanoplatelets are more vertically grown on the substrate. Similar types of nanoplates/nanodiscs with size/diameter of ~3 $\mu$m were obtained by Cao et al. using a chemical bath deposition[28] and by Gao et al. using a wet chemistry method.[29] Further increasing the deposition temperature to 50 °C (not shown) and 60 °C (Figure 1c) appear to substantially improve the alignment and vertical growth of the nanoplatelets, resembling nanowall structures (with similar thickness of 40−100 nm). Evidently, these nanowall structures not only are perpendicular to the substrate but also form groups of parallel nanowalls closely aligned in one direction. At a higher deposition temperature of 70 °C (Figure 1d), distinct nanowalls standing perpendicular to the substrate are clearly observed. These nanowalls are found to have well-defined ledges and sharp edges, with thickness remaining in the same range (40−100 nm). The growth of these nanowalls appears to be terminated at an angle by the presence of other nanowalls. It should be noted that when using a lower electrolyte concentration (0.05 M) but the same deposition temperature (70 °C), Xu et al. obtained random nanoplatelets with a discernibly larger thickness range of 70−400 nm.[26] Cao et al. also recently produced ZnO nanosheets by controlling the electrochemical currents, also at the lower electrolyte concentration of 0.05 M.[21,30] In these previous electrodeposition studies, the 2D ZnO nanostructures so obtained were mostly not perpendicular on the substrate. The perpendicular growth of nanowalls observed in the present work is believed to be due to our use of a higher electrolyte concentration (0.1 M) that leads to faster growth reaction kinetics. However, at the same electrolyte concentration (0.1 M), Chen et al. did not observe any 2D nanostructures, which might be caused by the use of a lower deposition potential.[18] This suggests that deposition parameters such as deposition temperature, potential, and time, as well as electrolyte concentration all play a crucial role interactively in controlling the morphology, alignment, uniformity, and perpendicular growth of ZnO nanowalls on the substrate. With increasing the deposition temperature to 80 °C, the nanowalls are found to become thicker (100−200 nm) and more closely packed, with a significant fraction appearing as merged nanowalls (Figure 1e). However, at the highest deposition temperature (90 °C) used in the present work, merging of the nanowalls appears to produce a patchy fibrillar film without any distinct nanowall structures, which might be due to the high turbulence of electrolyte during the deposition at a high temperature. We conclude that 70 °C corresponds to the optimum deposition temperature for electrochemically synthesizing individual well-defined ZnO nanowalls on ITO-glass in a 0.1 M electrolyte solution.

We show in Figure 2 more detailed SEM images of the nanowall structures obtained at 70 °C. In particular, distinct steps in the nanowalls (marked by arrows) (Figure 2a) and the smooth surface of nanowall ledges (Figure 2b) are clearly observed. Stacked (Figure 1d) and merged multiple nanowalls (Figure 2b) are also evident. Layer-by-layer stepped growth of ZnO nanosheets parallel to the substrate obtained by chemical vapor

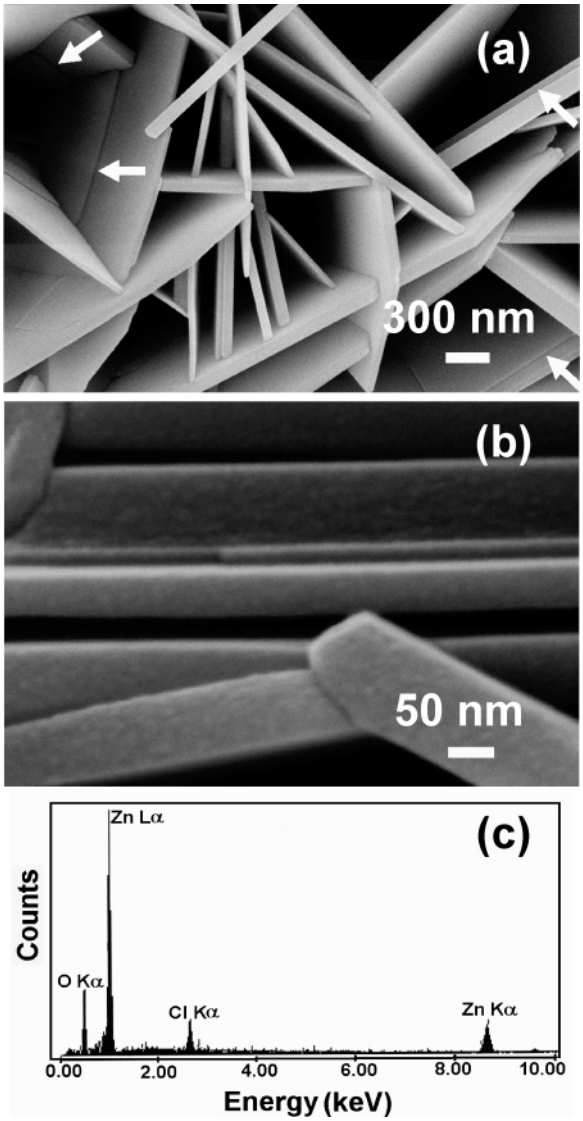


**Figure 2.** SEM images of ZnO nanowalls electrodeposited on ITO-glass at 70 °C, depicting (a) the single steps marked by arrows and (b) the smooth surface of the nanowall ledges. The corresponding EDX spectrum is shown in part c.

deposition has also been previously reported.[6] In contrast, we observe in the present work nanowalls either without steps or with only single steps, all of which are vertically grown. Moreover, vertical growth of nanowalls (with nanowires at the junctions of the nanowalls) has also been observed on a sapphire substrate in the presence of gold catalysts obtained by using thermal evaporation above 900 °C.[8,31] These walls are not flat and appear curved and flake-like and are continuous with an interconnecting quasi-3D honeycomb pattern. The thickness of the gold catalyst layer is found to be crucial in forming these nanowalls.[8,31] The present work therefore demonstrates that nanowalls can be obtained by electrodeposition at a considerably lower temperature, and these nanowalls are not only catalyst-free but also have distinct well-defined entities. Figure 2c shows the corresponding EDX spectrum of the as-deposited nanowalls, indicating the presence of Zn, O, and Cl. Similar EDX spectra (not shown) and atomic compositions are also obtained for the 2D nanostructures deposited at the other deposition temperatures. The presence of minor chlorine impurities is due to the supporting KCl electrolyte used in the electrochemical deposi-

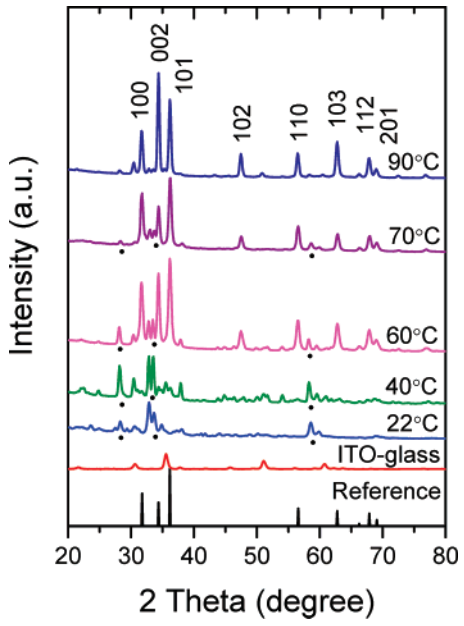


**Figure 3.** Evolution of GIXRD patterns of the 2D ZnO nanostructures electrodeposited on ITO-glass at different deposition temperatures. The crystallographic identifications of the prominent ZnO peaks are labeled, along with the bar chart of the reference ZnO powder (JCPDS 01-076-0704) and the pattern of ITO-glass substrate.

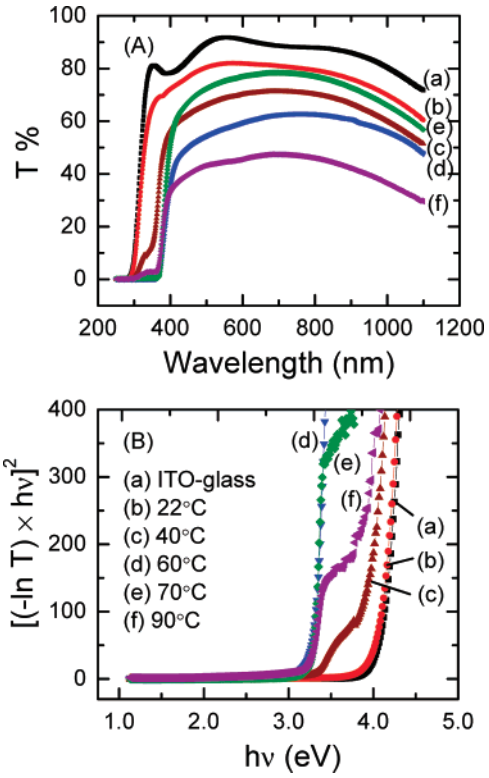


**Figure 4.** (A) Optical transmittance (*T*%) spectra and (B) the corresponding band gap spectra of ITO-glass electrodeposited (a) without and with 2D ZnO nanostructures at (b) 22, (c) 40, (d) 60, (e) 70, and (f) 90 °C.

tion process and is found to play an important role in the formation of the 2D nanostructures, as suggested in the earlier work.[26]

**3.2. Crystalline Phase Properties.** Figure 3 shows the GIXRD patterns of the 2D ZnO nanostructures obtained at different deposition temperatures, along with those of the ITO-glass substrate and a powder ZnO reference sample (JCPDS 01-076-0704).[32] Evidently, the 2D nanostructures obtained at 22, 40, and 50 °C (similar to those at 40 °C, not shown) do not exhibit XRD features of the ZnO wurtzite structure. However, the rather sharp and distinct XRD peaks from these samples indicate their highly crystalline phases. In particular, the prominent peaks near $2\theta = 28.3°$, 33.6°, 58.6° (marked with solid dots in Figure 3) are in reasonable correspondence to the XRD features of the leafy and thin platy ZnO crystals synthesized at 450 °C in an autoclave (JCPDS 00−021-1486, not shown).[33] The unassigned strong peak near $2\theta = 33.0°$ does not correspond to XRD features of any known ZnO phase or the ITO-glass substrate. This and the other unassigned peaks are possibly due to a new unknown ZnO phase, as also observed by Gao et al.,[29] or to some complexes formed in electrochemical deposition, as suggested by Izaki et al.[34] The GIXRD patterns of ZnO nanowalls obtained at 60, 70 (Figure 3), and 80 °C (not shown) are found to be very similar to one another, with the intensities of the leafy-phase XRD features[33] (marked by solid dots) found to be reduced for samples obtained at a higher deposition temperature. The major diffraction peaks for the nanowall samples [with calculated lattice constants of $a = b =$ 2.2497 (2.2533) Å, $c = 5.2096$ (5.2142) Å for the sample obtained at 70 °C (60 °C)] can be readily indexed (as labeled in Figure 3) to the wurtzite structure of ZnO (JCPDS 01-076-0704, with $a = b = 2.2530$ Å and $c = 5.2130$ Å).[32] Unlike the 1D ZnO nanostructures, which usually prefer growth in the (002) [or (0001)] plane,[1,11] the 2D ZnO structures have the strongest diffraction in the (101) [or $(10\bar{1}0)$] plane.[27,28,35] The present XRD results therefore indicate that a minimum deposition temperature of 60 °C is required to produce primarily wurtzite ZnO nanowalls. The GIXRD pattern of the sample deposited at 90 °C has also been found to correspond to the wurtzite phase, with the (002) peak being the most intense, which suggests the suppression of 2D growth. Furthermore, the relative intensities of the weak XRD features (not labeled in Figure 3) are found to be considerably reduced for samples obtained at deposition temperatures above 70 °C, indicating domination by the single-phase wurtzite structure at a higher deposition temperature.

**3.3. Optical Properties.** Figure 4A shows the transmittance (*T*%) spectra for the as-grown ZnO nanostructures deposited at various temperatures, along with that for the ITO-glass substrate. Assuming ZnO to be a typical direct-band-gap semiconductor,[19] the corresponding optical band gap can be estimated by the zero-crossing of the rising edge of the $(\alpha h\nu)^2$ vs $h\nu$ curve, where $h\nu$ is the photon energy and $\alpha$ ($= -\ln T$) is the absorbance, as shown in Figure 4B. As expected, all the ZnO deposited samples show lower *T*% than the ITO-glass substrate. Except for the lower transmittance, the spectrum of the nanosheets deposited at 22 °C (Figure 4A, curve b) appears similar to that of the ITO-glass substrate (Figure 4A, curve a), with both the band edge located at nearly the same wavelength of 280 nm (Figure 4A) and a band gap of 4.1 eV (Figure 4B). The observed band gap (4.1 eV) of the sample deposited at 22 °C corresponds to that of the ITO, which indicates that the band gap of the nanosheets, with a non-wurtzite ZnO phase as shown by our XRD results (Figure 3), is larger than 4.1 eV, in accord with the nonconducting nature of the sample due to the presence of $Zn(OH)_2$, as indicated by our XPS data (see below).

The transmittance spectra of ZnO deposited in the range of 50−90 °C (Figure 4A) are quite similar to one another, all of which with the band edge at 360 nm are in good accord with the corresponding values found for ZnO bulk single crystal[36] and for the electrochemically deposited ZnO thin films obtained by Izaki et al.[37] The nanowalls deposited at 70 °C appear to give the best *T*% in the visible region, suggesting that the

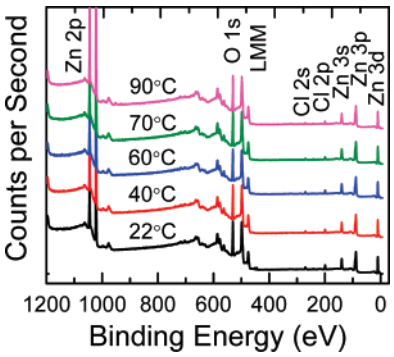


**Figure 5.** XPS survey spectra obtained after 3300 s of argon ion sputtering for 2D ZnO nanostructures electrodeposited on ITO-glass at 22, 40, 60, 70, and 90 °C. The spectra have been arbitrarily normalized at the Zn 3s peak position at 140.0 eV binding energy.

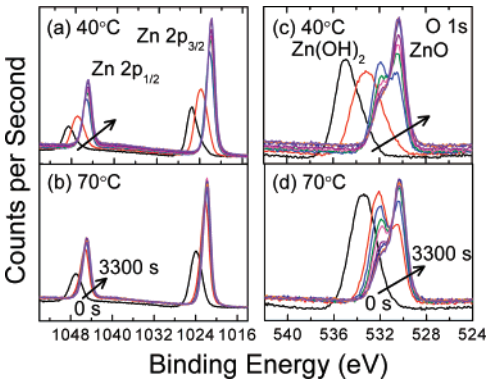


**Figure 6.** XPS spectra of (a, b) Zn 2p and (c, d) O 1s regions for 2D ZnO nanostructures deposited on ITO-glass at (a, c) 40 and (b, d) 70 °C and upon sputtering accumulatively for 0, 20, 60, 180, 300, 600, 900, 2100, and 3300 s.

crystallinity of the nanowalls deposited at 50 °C (not shown) and 60 °C (curve d) is poorer than that obtained at 70 °C (curve e). The lower *T*% observed for samples deposited at 80 (not shown) and 90 °C (curve f) could be due to the denser and thicker nature of these nanostructured films. The variations in *T*% of these ZnO nanostructures generally depend on their crystalline density, surface roughness, and defects in the samples.[38] It should be noted that the *T*% from the nanowalls obtained at 70 °C (77% at 600 nm) in the present work is higher than the ZnO nanopillar films electrochemically synthesized at the same temperature by Chen et al. (<50% at 600 nm).[18] This is consistent with the high crystalline quality found for the ZnO nanowalls obtained in the present work. The *T*% and the optical properties can be further enhanced by improving its crystallinity by postannealing these ZnO nanowalls synthesized at low temperature, as recently reported for electrochemically synthesized ZnO nanowires.[19] The nanowalls deposited at 50 °C (not shown) exhibit generally a lower *T*% but the same band edge (at 360 nm), suggesting that the ZnO leafy structures generally have a poorer crystallinity than the wurtzite structures of the nanowalls obtained at a higher deposition temperature. The corresponding band gaps for the ZnO nanowalls obtained at 60 (curve d) and 70 °C (curve e) are found to be 3.3 eV, which is the same as that of the bulk single crystal.[36] The good agreement in the band gaps found between the ZnO nanowalls obtained in the present work and that of the bulk single crystal therefore affirms their generally high crystal quality.

The transmittance spectrum of the nanoplatelets obtained at 40 °C (Figure 4A, curve c) appears to be intermediate between that of ITO (Figure 4A, curve a) and nanowalls (Figure 4A, curves d, e). In particular, the observed band edges (with the corresponding band gaps) at 300 (4.1 eV) and 342 nm (3.6 eV) are close to those of ITO at 297 nm (4.1 eV) and the Zn nanowalls at 370 nm (3.3 eV), respectively. These transmittance changes mark the evolution of the nanoplatelets into nanowalls and indicate that the leafy crystalline phase (Figure 3) found for the nanoplatelets has rather different optical properties from the wurtzite phase.

**3.4. X-ray Photoelectron Spectroscopy of ZnO Nanowalls.** The corresponding near-surface compositions of 2D ZnO nanostructures deposited at selected temperatures have been determined by XPS. In addition to the intense Zn 2p and O 1s features, the survey spectra of the as-deposited ZnO samples (not shown) also exhibit weak C and Cl features, which correspond to minor surface contamination and contributions from the KCl supporting electrolyte, respectively. Figure 5 shows the XPS survey spectra of ZnO samples collected from the bulk after argon ion sputtering for 3300 s. Although sputtering for 180−300 s was sufficient to remove the C features at the surface, the presence of the Cl features is found to persist throughout the sample, even upon sputtering for 3300 s, indicating that Cl is an integral part of the growth process. The peak positions of the corresponding prominent Zn $2p_{3/2}$ ($2p_{1/2}$) and O 1s features at 1021.7 (1044.8 eV) and 530.2 eV, respectively, are found to be in good accord with the reported literature values for ZnO.[39,40] The intensity ratios of the Zn $2p_{3/2}$ to O 1s features for the nanostructures appear to be independent of the deposition temperature, which suggests that the ZnO nanostructures are of the same composition.

The XPS spectral evolutions of the 2D ZnO nanostructures deposited at selected temperatures as a function of sputtering depth are found to be generally similar to one another. In Figure 6, we compare typical Zn 2p and O 1s spectra of ZnO nanoplatelets obtained at 40 °C and of nanowalls at 70 °C as functions of sputtering time. The single intense Zn $2p_{3/2}$ ($2p_{1/2}$) feature at 1021.7 eV (1044.8 eV) for both samples (Figure 6a, b) indicates the presence of only the divalent Zn(II) oxidation state, corresponding to both $Zn(OH)_2$ and ZnO. The observed spin−orbit splitting of 23.0 ± 0.1 eV is in good accord with the literature value of 22.97 eV.[41] The initial BE shift and the increase in the peak intensity of the Zn 2p features upon sputtering for the first 60 s is consistent with the presence of a $Zn(OH)_2$ overlayer. Furthermore, the corresponding single broad O 1s feature above 534 eV BE of the as-deposited nanostructures (Figure 6c,d) is also found to shift to a lower BE. Upon further sputtering, this broad O 1s feature evolves into two peaks at 531.8 and 530.2 eV, which correspond to $Zn(OH)_2$ and ZnO, respectively.[39,40] The measured BE difference of these two O 1s features (1.5 ± 0.1 eV) for the present samples and, indeed, all ZnO nanostructures obtained at different deposition temperatures in the present study is in good accord with the literature value of 1.5[42]−2.0 eV.[43] The fwhm of the O 1s $Zn(OH)_2$ feature (1.7−2.1 eV) is larger than that for the O 1s ZnO feature (1.3−1.5 eV), which is consistent with the amorphous nature of the $Zn(OH)_2$ component. Our fwhm values are also in good agreement with those reported for the ZnO films prepared by ion-gas layer reaction.[40]

Given that the nonconducting nature of $Zn(OH)_2$ is believed to produce differential charging that causes the BE shift, the larger BE shift observed for the as-deposited ZnO nanoplatelets (Figure 6a) could therefore be attributed to the presence of a higher $Zn(OH)_2$ mol % on the surface. The formation of $Zn(OH)_2$ at the surface is expected to occur naturally, considering that the electrochemical synthesis of ZnO involves an aqueous solution and subsequent washing of the sample in Millipore

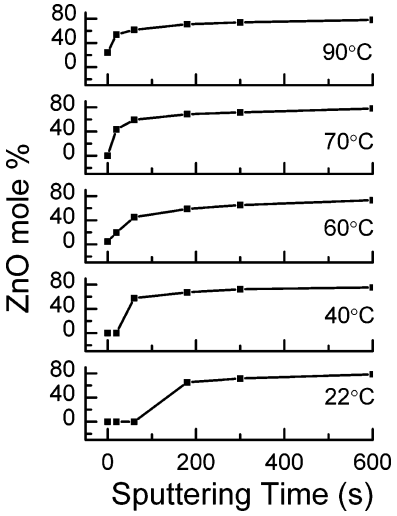


**Figure 7.** ZnO mol % as a function of total sputtering time for 2D ZnO nanostructures deposited on ITO-glass at 22, 40, 60, 70, and 90 °C.

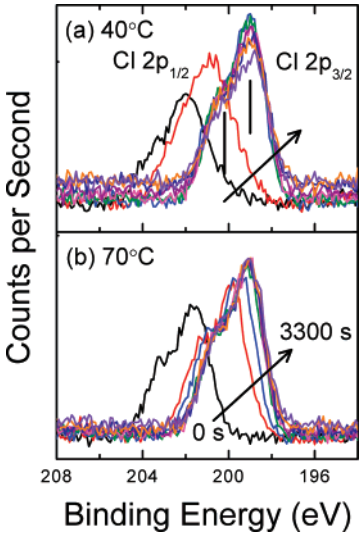


**Figure 8.** XPS spectra of Cl 2p region for 2D ZnO nanostructures electrodeposited on ITO-glass at (a) 40 and (b) 70 °C and upon sputtering accumulatively for 0, 20, 60, 180, 300, 600, 900, 2100, and 3300 s.

water. Moreover, in the commonly accepted mechanism of ZnO formation in a zinc nitrate electrolyte,[34,44] the $OH^-$ ions, produced in the reduction reaction of $NO_3^-$ to $NO_2^-$ ions, react with $Zn^{2+}$ ions to form the $Zn(OH)_2$ intermediate (i.e., the hydroxylation reaction) prior to the dehydration reaction of $Zn(OH)_2$ to ZnO. A certain quantity of residual $Zn(OH)_2$ could therefore remain without being completely converted to ZnO at the surface. As anticipated, the dehydration reaction is faster at a higher deposition temperature, enabling more complete conversion to ZnO and less residual $Zn(OH)_2$. This therefore leads to a smaller O 1s BE shift observed for the ZnO nanowalls deposited at 70 °C (Figure 6d) than the nanoplatelets at 40 °C (Figure 6c).

The mol % of ZnO in the electrodeposited sample can be estimated by the ratio of the area under the ZnO O 1s fitted curve to the sum of the ZnO O 1s fitted area and one-half of the $Zn(OH)_2$ O 1s fitted area. Figure 7 compares the relative changes of the ZnO mol % as a function of sputtering time for the 2D nanostructures deposited at different temperatures. After 300 s of sputtering, the ZnO mol % is found to level off at 75−80% for all the nanostructures, which is higher than the reported value of ZnO films deposited at 90 °C using an ion-gas layer reaction.[40] This suggests that a higher bulk ZnO composition can be achieved, even at a lower deposition temperature (≤70 °C), by electrodeposition, and it evidently does not depend on the morphology of the ZnO nanostructures. Furthermore, the onset of the ZnO mol % curves at a longer sputtering time found for the nanostructures obtained at a lower deposition temperature indicates a correspondingly thicker $Zn(OH)_2$ overlayer. The presence of a minor residual $Zn(OH)_2$ component (even after 3300 s of sputtering) suggests that $Zn(OH)_2$ cannot be completely eliminated, as demonstrated by Puchert et al., who detected both O 1s components, even on a ZnO single-crystal surface freshly cleaved under vacuum, and attributed its presence to rapid surface hydroxylation.[39]

In addition to the prominent Zn and O features, the presence of minor Cl features is also observed throughout all the ZnO nanostructures. Figure 8 compares the corresponding Cl 2p XPS spectra obtained as a function of sputtering time for the ZnO nanoplatelets deposited at 40 °C and nanowalls at 70 °C. The Cl 2p envelope (consisting of the Cl $2p_{3/2}$ at 199.0 eV and Cl $2p_{1/2}$ at 200.6 eV obtained after 3300 s sputtering) is found to be shifting toward the lower BE due to the removal of the $Zn(OH)_2$ overlayer upon sputtering. The initial shift observed for the nanoplatelets (Figure 8a), which is larger than that for the nanowalls (Figure 8b), is consistent with the presence of a larger $Zn(OH)_2$ surface component in the nanostructures obtained at a lower deposition temperature. Furthermore, the initial BE shift and the increase in the peak intensity of the Cl 2p envelope upon sputtering observed for all the samples are consistent with the presence of a $Zn(OH)_2$ overlayer and with Cl playing an integral role in the 2D nanostructure growth of ZnO.

**3.5. Growth Mechanism of Nanowalls.** The mechanism of the electrochemical formation of ZnO from zinc nitrate in an aqueous solution is well-known.[34] Briefly, the dissociation of zinc nitrate produces $Zn^{2+}$ and $NO_3^-$ ions, the latter of which subsequently reduces to $NO_2^-$ ions. The resulting $OH^-$ ions react with the $Zn^{2+}$ ions to produce $Zn(OH)_2$ in the hydroxylation reaction, which then undergoes a dehydration reaction to ZnO. However, due to the faster growth rate along the $[10\bar{1}0]$ and $[2\bar{1}\bar{1}0]$ directions and of the ±(0001) polar surfaces of ZnO, the growth can produce a large variety of nanostructures, depending on the deposition parameters.[5]

In the present work, a separate set of experiments has been carried out to understand the growth behavior of ZnO nanowalls on ITO-glass substrate. Figure 9 shows the morphology evolution of the ZnO nanowalls deposited at 70 °C as a function of deposition time. For the 1 s deposition, ZnO forms predominantly as spherical particles (Figure 9a), with a few taking elongated shape and appearing as nanobars (Figure 9b). With an increase in the total deposition time to 30 s, the ZnO nanobars become nanoplatelets, growing either parallel or perpendicular to the substrate (Figure 9c, d). A large number of ZnO nanoplatelets are found to be hexagonal in shape. Some of these platelike structures appear to grow as bunches or clusters. Further increasing the total deposition time to 60 s leads to almost all nanoplatelets taking the shape of hexagonal disks, with a large fraction becoming more upright (Figure 9e,f). In contrast to the previous work on ZnO nanoplatelets that require longer deposition times (exceeding 1 h),[21,26,29] the present work shows that a faster formation of ZnO nanoplatelets, in just 60 s, can be achieved by electrodeposition in a more concentrated electrolyte. At a total deposition time of 300 s, the deposited ZnO nanoplatelets/disks lose their hexagon shape and become well-defined nanowalls of length 1−2 $\mu$m (Figure 9g, h). The

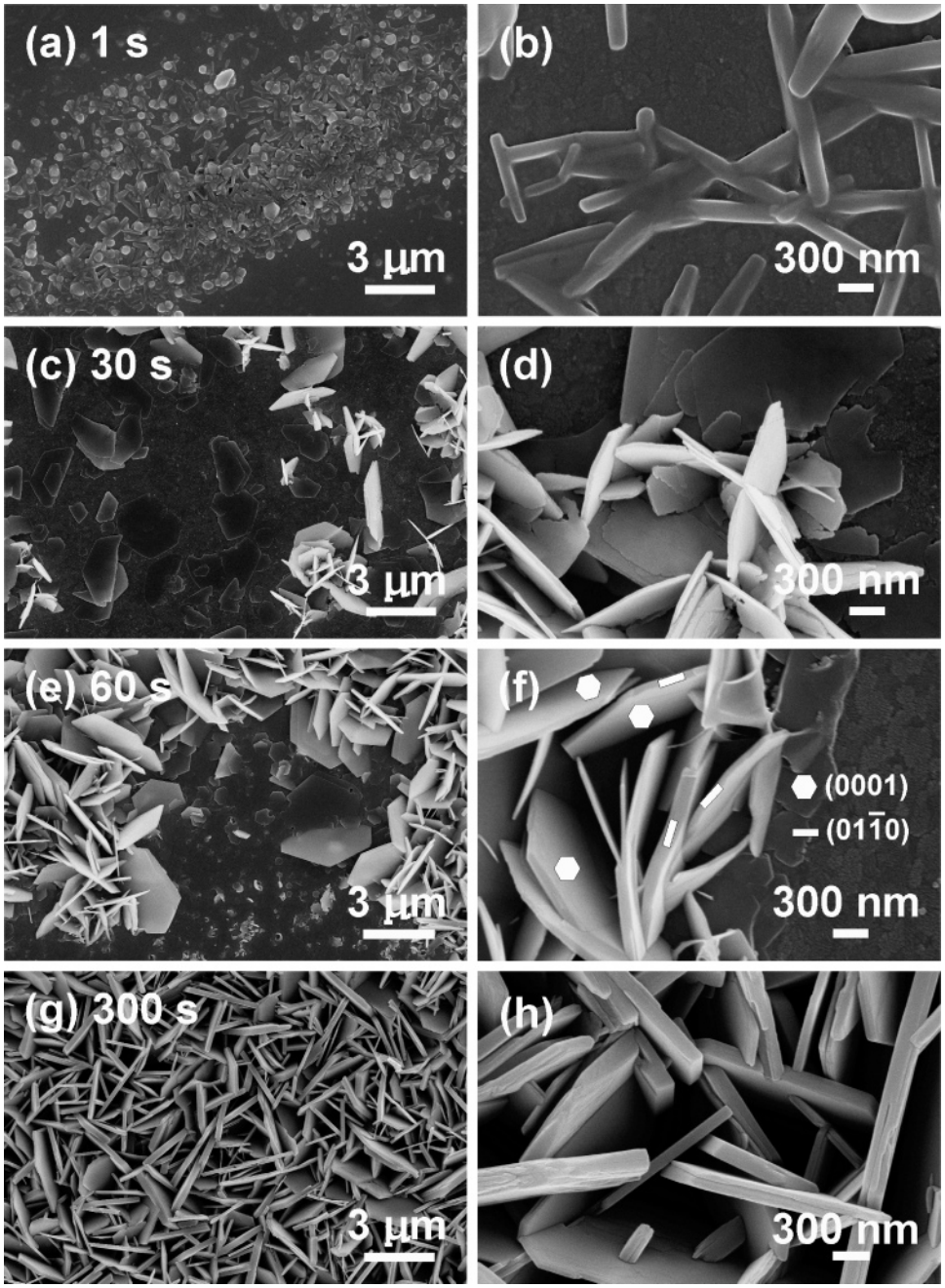


**Figure 9.** SEM images of 2D ZnO nanostructures electrodeposited at 70 °C on ITO-glass for a total deposition time of (a, b) 1, (c, d) 30, (e, f) 60, and (g, h) 300 s.

growth of these nanowalls in the lateral direction appears to cease when one nanowall meets another, whereas their height increases with increasing deposition time without substantial change in the wall thickness.

Figure 10 shows a schematic diagram of the ZnO nanowall formation. The growth direction of ZnO nanorods is known to be along the *c*-axis, that is, in the (0001) plane, while the 2D structures prefer to grow in the (10$\bar{1}$0) and (2$\bar{1}\bar{1}$0) planes.[45,46] In the case of electrochemical deposition, the electrolyte concentration and its constituents determine the growth direction and the subsequent formation of nanostructures. The TEM study by Yoshida et al. indicated that the preferential growth of the stacking ZnO disk in the (10$\bar{1}$0) plane was due to adsorption of tetrasulfonated metallophthalocyanines onto the (0001) plane of ZnO.[24] Xu et al. further observed growth of ZnO nanoplates by using a less concentrated electrolyte solution (of $Zn(NO_3)_2$ mixed with KCl) and suggested that the $Cl^-$ ions may act as a

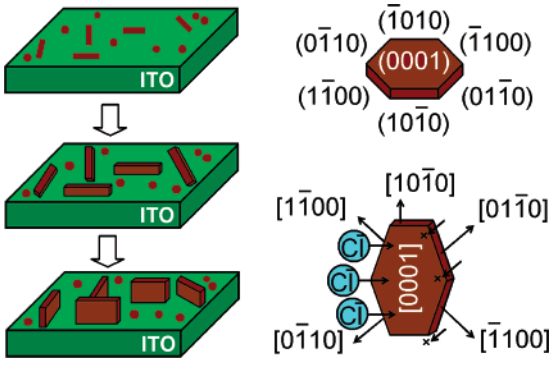


**Figure 10.** Schematic diagram of a plausible growth mechanism of ZnO nanowalls.

capping agent that hinders the growth in the (0001) plane.[26] In the present work, we demonstrate for the first time the presence

of $Cl^-$ ions throughout the 2D ZnO nanostructures by the respective XPS depth profile (Figure 9). In a separate experiment without the use of KCl supporting electrolyte, we obtained ZnO nanopillars, and no 2D nanostructure was found. These results therefore validate the role of $Cl^-$ ions as the capping agent for the (0001) plane in the formation mechanism of nanowalls (Figure 10). The difference in the morphology of the nanostructures reported by Xu et al.[26] (nanoplates) and the present work (nanowalls) could be attributed to differences in the electrolyte concentration. A high electrolyte concentration of both $Zn(NO_3)_2$ and KCl (0.1 M) and the use of an optimum deposition potential (−1.1 V) and deposition temperature (70 °C) is therefore crucial in producing distinct nanowalls, as shown in the present work. Furthermore, it is possible to control the thickness and height (and their alignment) of the nanowalls by further fine-tuning the electrolyte concentrations and by changing the deposition time, respectively.

## 4. Conclusions

Two-dimensional ZnO nanostructures have been deposited on ITO-glass by using electrochemical deposition. The deposition temperature is found to play an important role in controlling the morphologies, shapes, and crystalline phases of these 2D ZnO nanostructures. In particular, the morphology of the nanostructures changes from randomly oriented, poorly crystalline nanosheets at 22 °C to well-aligned nanowalls at 70 °C. At 80 °C, nanowalls are found to merge with one another, and they become patchy fibrillar structures at 90 °C. Although ZnO nanostructures deposited below 50 °C exhibit crystalline character corresponding to the leafy ZnO phase, the wurtzite phase is observed only from the ZnO nanostructures obtained at a higher deposition temperature (nanowalls at 60−80 °C and patchy nanostructures at 90 °C). In addition, the ZnO nanostructures deposited at 50−90 °C show an optical band gap (3.3 eV) identical to that for the single-crystal ZnO, confirming their high crystal quality. Their transmittance is also found to vary from 40 to 75% depending upon the morphologies of samples. Detailed XPS depth-profile measurements show that the ZnO nanostructures are covered by a $Zn(OH)_2$ overlayer, in good accord with the general growth model that involves $Zn^{2+}$ hydroxylation followed by dehydration to ZnO. The presence of chlorine throughout the ZnO nanostructures is also observed, which verifies for the first time its role as a capping agent in the 2D growth mechanism that hinders ZnO growth in the (0001) plane, thereby permitting growth in the $(10\bar{1}0)$ plane. By changing the deposition time at 70 °C, we also illustrate the early formation of nanowalls, from nanoparticles to 1D nanobars to largely nonvertical 2D nanoplatelets and, finally, to near-perpendicular 2D nanowalls.

**Acknowledgment.** This work was supported by the Natural Sciences and Engineering Research Council of Canada.

## References and Notes

(1) Zang, J.; Li, C. M.; Cui, X.; Wang, J.; Sun, X.; Dong, H.; Sun, C. Q. *Electroanalysis* **2007**, *19*, 1008.

(2) Huang, M. H.; Mao, S.; Feick, H.; Yan, H.; Wu, Y.; Kind, H.; Weber, E.; Russo, R.; Yang, P. *Science* **2001**, *292*, 1897.

(3) Ravirajan, P.; Peiro, A. M.; Nazeeruddin, M. K.; Graetzel, M.; Bradley, D. D. C.; Durrant, J. R.; Nelson, J. *J. Phys. Chem. B* **2006**, *110*, 7635.

(4) Wang, W.; Zeng, B.; Yang, J.; Poudel, B.; Huang, J.; Naughton, M. J.; Ren, Z. *Adv. Mater.* **2006**, *18*, 3275.

(5) Gao, P. X.; Lao, C. S.; Ding, Y.; Wang, Z. L. *Adv. Funct. Mater.* **2006**, *16*, 53 and references therein.

(6) Chen, S.; Liu, Y.; Shao, C.; Mu, R.; Lu, Y.; Zhang, J.; Shen, D.; Fan, X. *Adv. Mater.* **2005**, *17*, 586.

(7) Li, F.; Ding, Y.; Gao, P. X.; Xin, X.; Wang, Z. L. *Angew. Chem. Int. Ed.* **2004**, *116*, 5350.

(8) Ng, H. T.; Li, J.; Smith, M. K.; Nguyen, P.; Cassell, A.; Han, J.; Meyyappan, M. *Science* **2003**, *300*, 1249.

(9) Gao, P. X.; Song, J.; Liu, J.; Wang, Z. L. *Adv. Mater.* **2007**, *19*, 67.

(10) Lu, C.; Qi, L.; Yang, J.; Tang, L.; Zhang, D.; Ma, J. *Chem. Commun.* **2006**, 3551.

(11) Kar, S.; Dev, A.; Chaudhuri, S. *J. Phys. Chem. B* **2006**, *110*, 17848.

(12) Fan, Z.; Dutta, D.; Chien, C. J.; Chen, H. Y.; Brown, E. C.; Chang, P. C.; Lu, J. G. *Appl. Phys. Lett.* **2006**, *89*, 213110.

(13) Peulon, S.; Lincot, D. *Adv. Mater.* **1996**, *8*, 166.

(14) Lao, J. Y.; Huang, J. Y.; Wang, D. Z.; Ren, Z. F.; Steeves, D.; Kimball, B.; Porter, W. *Appl. Phys. A* **2004**, *78*, 539.

(15) Liu, B.; Zeng, H. C. *J. Am. Chem. Soc.* **2004**, *126*, 16744.

(16) Tian, Z. R.; Voigt, J. A.; Liu, J.; Mckenzie, B.; McDermott, M. J.; Rodriguez, M. A.; Konishi, H.; Xu, H. *Nat. Mater.* **2003**, *2*, 821.

(17) Pauporte, T.; Lincot, D.; Viana, B.; Pelle, F. *Appl. Phys. Lett.* **2006**, *89*, 233112.

(18) Chen, Q. P.; Xue, M. Z.; Sheng, Q. R.; Liu, Y. G.; Ma, Z. F. *Electrochem. Solid State Lett.* **2006**, *9*, C58.

(19) Anthony, S. P.; Lee, J. I.; Kim, K. J. *Appl. Phys. Lett.* **2007**, *90*, 103107.

(20) Levy-Clement, C.; Tena-Zaera, R.; Ryan, M. A.; Katty, A.; Hodes, G. *Adv. Mater.* **2005**, *17*, 1512.

(21) Cao, B.; Teng, X.; Heo, S. H.; Li, Y.; Cho, S. O.; Li, G.; Cai, W. *J. Phys. Chem. C* **2007**, *111*, 2470.

(22) Yang, J.; Liu, G.; Lu, J.; Qiu, Y.; Yang, S. *Appl. Phys. Lett.* **2007**, *90*, 103109.

(23) Wong, M. H.; Berenov, A.; Qi, X.; Kappers, M. J.; Barber, Z. H.; Illy, B.; Lockman, Z.; Ryan, M. P.; MacManus-Driscoll, J. L. *Nanotechnology* **2003**, *14*, 968.

(24) Yoshida, T.; Tochimoto, M.; Schlettwein, D.; Woehrle, D.; Sugiura, T.; Minoura, H. *Chem. Mater.* **1999**, *11*, 2657.

(25) Illy, B.; Shollock, B. A.; MacManus-Driscoll, J. L.; Ryan, M. P. *Nanotechnology* **2005**, *16*, 320.

(26) Xu, L.; Guo, Y.; Liao, Q.; Zhang, J.; Xu, D. *J. Phys. Chem. B* **2005**, *109*, 13519.

(27) Peng, Y.; Xu, A.; Deng, B.; Antonietti, M.; Coelfen, H. *J. Phys. Chem. B* **2006**, *110*, 2988.

(28) Cao, B.; Cai, W.; Li, Y.; Sun, F.; Zhang, L. *Nanotechnology* **2005**, *16*, 1734.

(29) Gao, Y.; Nagai, M. *Langmuir* **2006**, *22*, 3936.

(30) Cao, B.; Cai, W.; Zeng, H.; Duan, G. *J. Appl. Phys.* **2006**, *99*, 73516.

(31) Kim, S.-W.; Park, H.-K.; Yi, M.-S.; Park, N.-M.; Park, J.-H.; Kim, S.-H.; Maeng, S.-L.; Choi, C.-J.; Moon, S.-E. *Appl. Phys. Lett.* **2007**, *90*, 033107.

(32) PDF-2 Database, International Center for Diffraction Data (ICDD), 2004.

(33) Bauer, R. *Krist. Tech.* **1968**, *3*, 375.

(34) Izaki, M.; Omi, T. *J. Electrochem. Soc.* **1996**, *143*, L53.

(35) Xi, Y.; Hu, C. G.; Han, X. Y.; Xiong, Y. F.; Gao, P. X.; Liu, G. B. *Solid State Commun.* **2007**, *141*, 506.

(36) Gray, D. E. *American Institute of Physics Handbook*, 3rd ed.; AIP: New York, 1972: pp 9−24.

(37) Izaki, M.; Omi, T. *Appl. Phys. Lett.* **1996**, *68*, 2439.

(38) Yamamoto, T.; Shiosaki, T.; Kawabata, A. *J. Appl. Phys.* **1980**, *51*, 3113.

(39) Puchert, M. K.; Timbrell, P. Y.; Lamb, R. N. *J. Vac. Sci. Technol., A* **1996**, *14*, 2220.

(40) Bär, M.; Reichardt, J.; Sieber, I.; Grimm, A.; Kötschau, I.; Lauermann, I.; Sokoll, S.; Lux-Steiner, M. C.; Fischer, C. H.; Niesen, T. P. *J. Appl. Phys.* **2006**, *100*, 23710.

(41) Moulder, J. F.; Stickle, W. F.; Sobol, P. E.; Bomben, K. D. *Handbook of X-ray Photoelectron Spectroscopy*; Chastain, J., Ed.; Perkin-Elmer Corporation, U.S.A.: Waltham, MA, 1992.

(42) Deroubaix, G.; Marcus, P. *Surf. Interface Anal.* **1992**, *18*, 39.

(43) Au, C. T.; Roberts, M. W.; Zhu, A. R. *Surf. Sci.* **1982**, *115*, L117.

(44) Pauporte, T.; Lincot, D. *J. Electrochem. Soc.* **2001**, *148*, C310.

(45) Wei, Q.; Meng, G.; An, X.; Hao, Y.; Zhang, L. *Nanotechnology* **2005**, *16*, 2561.

(46) Pan, Z. W.; Dai, Z. R.; Wang, Z. L. *Science* **2001**, *291*, 1947.